Microchemical Journal 198 (2024) 110186

Contents lists available at ScienceDirect

Microchemical Journal

journal homepage: www.elsevier.com/locate/microc

Determination of ofloxacin in urine using UV/Vis absorption spectroelectrochemistry

Fabiola Olmo, Alvaro Colina *, Aranzazu Heras *

Department of Chemistry, Universidad de Burgos, Plaza Misael Bañuelos, s/n, E-09001 Burgos, Spain

ARTICLE INFO

Keywords:
Ofloxacin
Urine
Spectroelectrochemistry
Multivariate analysis

ABSTRACT

UV–Vis absorption spectroelectrochemistry has been selected as a suitable multiresponse technique to determine the fluoroquinolone ofloxacin in urine samples without any previous pretreatment. Due to the modification of the working electrode surface during the oxidation of this antibiotic, the electrode has to be replaced or polished between measurements. A new spectroelectrochemistry cell has been developed, which allows in an simple way to perform reproducible experiments with different screen-printed electrodes. The new cell has been used to perform analysis in a complex matrix such as urine. Due to the trilinear character of the spectroelectrochemical data, PARAFAC has been used to determine ofloxacin with very good figures of merit, demonstrating the capability of trilinear methods to avoid the influence of some interfering compounds.

1. Introduction

Quinolones and, in particular, fluoroquinolones (FQs) are a family of synthetic antibiotics with a high antibacterial activity and relevant pharmacokinetic properties [1,2]. The basic FQ structure consists of a bicyclic core with a N in carbon 1, a carboxyl group at carbon 3, a carbonyl group at carbon 4, and a fluorine atom at carbon 6 of the quinolone scaffold [3]. FQs are commonly prescribed to treat bacterial infections caused by both Gram-positive and Gram-negative bacteria, including, among others, urinary tract infections, sexually transmitted diseases, tuberculosis, pneumonia, and skin and soft tissue infections. These antibiotics inhibit bacterial RNA and DNA synthesis through the formation of a quinolone-enzyme-DNA complex that blocks the catalytic activity of DNA gyrase and topoisomerase IV, causing cell and bacterial death [4–6].

Ofloxacin (OFL) is considered a second generation FQ with a N-methylpiperazine group attached to carbon 7, widely used in the treatment of respiratory, digestive and urinary tract infections against Gram-negative bacteria in both humans and animals [1,2,7–9]. However, despite its great potential to address various bacterial infections, OFL is under surveillance. The World Health Organization and National Academy of Medicine in the United States of America are currently concerned about the prevalence of trace amounts of FQs in the environment [2]; in particular, a large concentration of OFL has been detected in many aquatic environments. It is estimated that 70–80 % of ingested OFL is excreted unmetabolized via urine to domestic wastewater and sewage treatment plants [10]. Overexposure to OFL-contaminated waters leads to adverse reactions in the human body and results in multiple ecosystem and environmental problems, such as microbial resistance [11–13].

To date, liquid chromatography, mass spectrophotometry, UV–Vis spectrometry and fluorescence represent the most relevant techniques to study OFL [7,9,14–16]. Nevertheless, the application of these techniques usually requires the use of expensive instrumentation and complex working protocols. Overcoming the main problems of these techniques, the development of electrochemical sensors has led to simpler methods that allow the study and detection of this type of molecules. Despite the great advantages of electrochemical methods such as simplicity, quickness, sensitivity and reproducibility, it is often necessary to carry out prior optimization work or even the development of specific modified electrodes to improve the selectivity and/or sensitivity [7–9,14–20].

In this work, spectroelectrochemistry (SEC) is proposed to develop a working protocol that allows the quantification of OFL in a complex

Abbreviations: OFL, ofloxacin; FQ, fluoroquinolones; UA, uric acid; SEC, spectroelectrochemistry; UV–Vis SEC, UV–Vis absorption spectroelectrochemistry; SPE, screen printed electrode; CE, counter electrode; WE, working electrode; RE, pseudo-reference electrode; CV, cyclic voltammogram; OCP, open circuit potential; CVA, cyclic voltabsorptogram; DVA, derivative voltabsorptogram; MAD, multipulsed amperometric detection.

* Corresponding authors.
E-mail addresses: acolina@ubu.es (A. Colina), maheras@ubu.es (A. Heras).

https://doi.org/10.1016/j.microc.2024.110186
Received 12 December 2023; Received in revised form 15 February 2024; Accepted 17 February 2024
Available online 18 February 2024

media in a simple and reproducible way. The specific photophysical properties of OFL, such as its characteristic absorption spectra, its acid-base behavior and the possibility of electrochemical oxidation, make it a perfect candidate to be studied by SEC techniques, as in this case UV–Vis absorption SEC (UV–Vis SEC). This technique, which provides two signals of different nature but fully correlated, one electrochemical and other spectroscopic, is increasingly used in chemical analysis, characterization of new materials or in the study of electrochemical processes [21]. Considering that a light beam can interrogate the diffusion layer in different ways, a distinction is made between two optical arrangements known as normal configuration and parallel configuration [22]. In this work, since OFL can be detected in the solution adjacent to the electrode surface, a parallel configuration respect to the electrode surface is chosen, aligning two optical fibers on the working electrode (WE) surface to record all the changes taking place during the OFL oxidation process. Usually, the SEC cells described in literature based on optical fibers, fix them directly on the surface of the working electrode [23]. However, an experimental set-up based on fixed optical fibers on the WE entails certain problems which must be overcome. For example, when the generated product is adsorbed on the WE surface the set-up is not useful because a different electrode is required for each measurement [23]. In that case, the optical fibers must be fixed to a new electrode after each measurement and, consequently, the distance between the fibers may change, affecting the optical path length and losing the necessary reproducibility within the set of experiments [23].

Some alternatives have been proposed to overcome this drawback such as aligning and fixing the optical fibers on a quartz plate subsequently placed on the working electrode, which allows the electrode change while maintaining the optical path [21]. This set-up involves working in a thin-layer regime, since the solution is confined in a small space, which can be very useful in the quantification field as total electrolysis of the analyte occurs [21]. However, for other processes, such as the study of reaction mechanisms, it may be more convenient to work under semi-infinite diffusion conditions. In this work, a new SEC cell has been developed, which allows changing the electrode without modifying the optical pathway, obtaining very reproducible experiments in the semi-infinite diffusion regime. The new SEC cell allows us to follow and study processes that modify the electrode surface and the electrode can be changed easily in a very reproducible way, without modifying the optical path-length, which is mandatory for analytical purposes.

Finally, time-resolved SEC experiments provide a large amount of data which can be used to resolve complex problems, especially when the determination of an analyte is carried out in a complex matrix. The trilinear character of SEC data allows us to use powerful chemometric tools for quantification of FQs, particularly OFL, in real matrices such as urine samples. The presence of potential interfering compounds in the determination of OFL is a significant problem, because it can undoubtedly affect the quantification of this antibiotic, compromising the validity of the obtained results.

Therefore, the main objective of this work is to quantify OFL in a real urine sample using a new UV–Vis SEC cell working in parallel configuration and using PARAFAC as chemometric tool to extract the quantitative information of the SEC data set. The development of methodologies for the quantification of these drugs in urine can help to determine the efficiency of medical treatments and to optimize the appropriate dose to be administered to the patient.

2. Experimental section

2.1. Reagents and materials

Ofloxacin (OFL, Sigma-Aldrich) and uric acid (UA, ACS reagent, Acros Organics), were used as received without further purification. All solutions were prepared in 0.1 M KCl (Acros Organics) and in 0.1 M Britton-Robinson (BR) as the supporting electrolyte, being the final pH of this solution 4.02. This buffer solution contains boric acid (H_3BO_3, PANREAC), phosphoric acid (H_3PO_4, 85 %, PANREAC), acetic acid (HAc, VWR Chemicals) and sodium hydroxide (NaOH, Acros Organics).

All these solutions were prepared using high-quality ultrapure deionized water (18.2 MΩ cm resistivity at 25 °C, Milli-Q Direct 8, Millipore) and the final pH of the solution was measured with a pH electrode (sensION). All experiments were performed at room temperature.

2.2. Instrumentation and software

UV–Vis SEC experiments were performed using a customized SPELEC instrument (Metrohm-DropSens) controlled by DropView SPELEC software (Metrohm-DropSens). This instrument includes a potentiostat/galvanostat, a spectrometer, and a halogen-deuterium light source.

In addition, a SEC cell was designed and fabricated to carry out the experimental work. A detailed description of the SEC cell is given in Section 2.3. Moreover, a new carbon screen printed electrode (SPE, DRP-110, Metrohm-DropSens) was used in each SEC measurement. These SPEs consist of a 4 mm diameter disc screen printed carbon working electrode (WE), a carbon counter electrode (CE) and a silver pseudo-reference electrode (RE). Two bare optical fibers (100 μm, Ocean Optics) were used to illuminate the sample and to collect the light beam, which is conducted to the spectrometer.

2.3. Design and fabrication of the SEC cell

As previously explained, adsorption of the reaction product on the WE surface causes the modification of the electrode, leading to changes in both the electrochemical and the spectroscopic responses. Therefore, the use of a new electrode after each experiment is essential. In addition, in parallel UV–Vis SEC, working with a fixed and known optical-pathway length during a set of experiments is mandatory. With all these factors in mind, a new parallel UV–Vis SEC cell that works in semi-infinite regime has been developed, allowing the replacement of the SPE without modifying the optical-pathway length in a very easy and reproducible way. For this purpose, the optical fibers were fixed and aligned directly on the upper body of the cell, instead of on the WE. In this way, the quantification of OFL is simplified.

Fig. 1a shows the SEC cell, which consists of two different bodies with four 5 mm holes positioned at each corner where magnets are placed, which allow a reproducible magnetic fixation. The lower body has been designed and created with a 3D printer (Photon Mono SE, ANYCUBIC) using UV sensitive 405 nm resin (ANYCUBIC), while the upper body was fabricated in poly(methyl methacrylate) (PMMA) using a high-precision CO_2 laser cutting machine. The lower body measures 65.0 × 40.0 × 8.0 mm and features a rectangular space (29 × 10 mm) to insert the SPE, as well as a small opening to connect the SPE to the potentiostat. The upper body measures 47.5 × 40.0 × 9.8 mm and features a circular cavity of 16 mm in diameter with two small 2.6 mm diameter pillars to support the optical fibers. These pillars facilitate the alignment of the optical fibers at different optical path lengths, as can be observed in the Fig. 1b. The circular cavity allows working in semi-infinite regime during the SEC experiments. In this way, the light beam passes close to the WE surface in parallel configuration and is conducted to the spectrometer, which collects the absorbance changes occurring in the solution adjacent to the WE.

In summary, the home-made UV–Vis SEC cell described above has been optimized to perform experiments in parallel configuration and in a semi-infinite diffusion regime in a simple and reproducible way. Additionally, the replacement of the SPE between experiments without altering the optical path length is facilitated.

2.4. Experimental set-up for SEC measurements

In all the experiments carried out in this work, the light beam

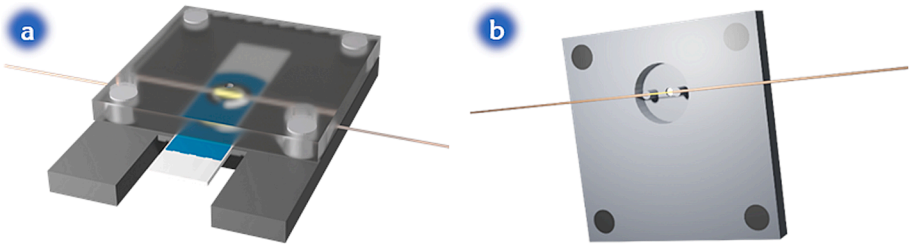

Fig. 1. (a) Schematic image of the parallel UV–Vis SEC cell to work in semi-infinite diffusion regime, and (b) detailed schematic view of the upper body of the cell.

interrogates the solution in a parallel direction to the WE surface. For this purpose, two 100 μm bare optical fibers were aligned and fixed with nail polish in the upper piece on the two pillars described in Fig. 1. One of these fibers is coupled to the light source while the other one is connected to the spectrometer. The optical pathway is the distance between the two optical fibers, which is measured using ImageJ [24], obtaining in this set of experiments a value of 2.07 mm.

To perform the parallel UV–Vis SEC experiments, the SPE is first placed in the lower body and 50 μL of the test solution is added, making sure that the drop completely covers the three electrodes of the SPE. Then, the upper body with the optical fibers is perfectly attached to the lower part, thanks to the four magnets present in the corners of both pieces. Finally, the SPE is connected to the potentiostat.

3. Results and discussion

The main objective of this work is to measure OFL levels in real urine samples. It should be noted that urine is a complex matrix containing potentially interfering compounds. One of the most common compounds found in urine is uric acid (UA), which can be also oxidized. For these reason, before starting a complex analysis, the individual study of the UV–Vis SEC behavior of both OFL and UA has been carried out.

3.1. OFL study by UV–Vis SEC

First, a 100 μM OFL solution in 0.1 M KCl and BR buffer (pH = 4.02) was measured by performing cyclic voltammetry between +0.70 V and +1.10 V at 0.01 V·s^{-1}. Fig. 2a shows the cyclic voltammogram (CV), where an anodic peak related to the oxidation of OFL evolves around +0.99 V. During the backward scan, no reduction peak is observed, indicating that the oxidation of OFL is an irreversible process. Concomitantly, the evolution in the UV–Vis absorption spectra was recorded every 10 ms. The corresponding contour map of the spectra during the experiment is shown in Fig. 2b. It should be noted that the UV–Vis absorption spectrum of OFL at OCP was taken as reference, so the spectral changes occurred during the cyclic voltammetry experiment were recorded. The oxidation of OFL leads to the evolution of three absorption bands. One increases with the applied potential at 245 nm

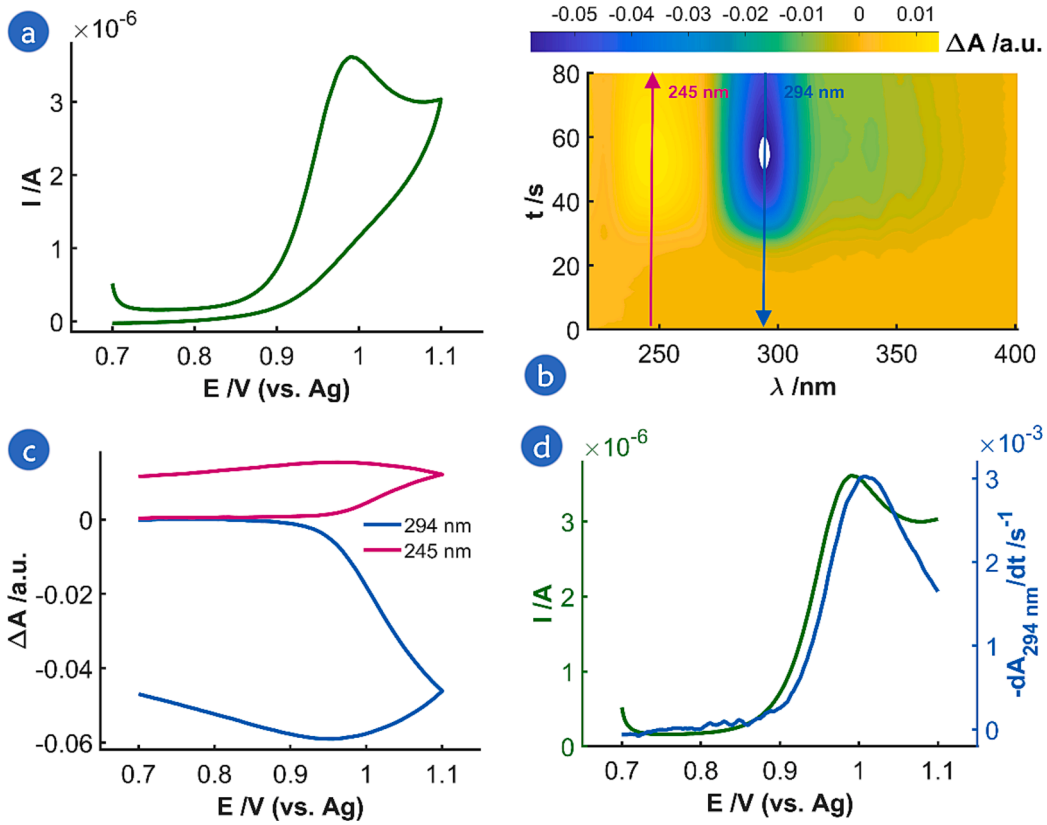

Fig. 2. SEC experiment of 100 μM OFL in BR buffer (pH = 4.02) and 0.1 M KCl between +0.70 V and +1.10 V at 0.01 V·s^{-1}. (a) CV, (b) contour plot with spectra evolution during the potential scan (pink arrow: band at 245 nm, blue arrow: band at 294 nm), (c) CVA at 245 nm (pink line) and 294 nm (blue line), (d) comparison of CV (green line) and DVA at 294 nm (blue line). (For interpretation of the references to colour in this figure legend, the reader is referred to the web version of this article.)

being related to the generation of the oxidized form of OFL. The strong absorption band that decreased at 294 nm corresponds to a $\pi \rightarrow \pi^*$ transition of the chromophore involving from the N-1 position to the carboxylic acid group; on the other hand the weak absorption band at 340 nm is linked to the $n \rightarrow \pi^*$ transition of the chromophore involving the nitrogen of the piperazinyl group to the carbonyl group [25,26]. Both absorption bands with a negative behavior are associated to the consumption of OFL during the oxidation process. The cyclic voltabsorptograms (CVAs, Fig. 2c) show the evolution of the absorbance at 294 nm and 245 nm with the applied potential. From +0.90 V onwards in the anodic scan, an abrupt change in absorbance occurs, which corresponds to the oxidation process of OFL shown in Fig. 2a. The derivative voltabsorptogram (DVA) at 294 nm, Fig. 2d, shows the correlation between the electrochemical and spectroscopic signals, demonstrating that both responses are only related to the oxidation of OFL.

3.2. UA study by UV–Vis SEC

Similarly, a comparable analysis was carried out in a 100 μM UA in 0.1 M KCl and BR buffer (pH = 4.02) solution. In this case, the CV recorded between 0.00 V and +0.70 V at 0.01 $V \cdot s^{-1}$ is also characterized by a single anodic peak around +0.45 V (Fig. S1a) assigned to the irreversible oxidation process of UA. The evolution of the UV–Vis absorption spectra recorded simultaneously every 10 ms (Fig. S1b), taking the initial UA solution as reference spectrum, displays two absorption bands that decrease during the anodic scan. These spectra are defined by a weak negative band at 237 nm and a more intense band at 286 nm, both related to the depletion of UA in solution [27,28]. The CVAs at 237 and 286 nm, represented in Fig. S1c, show that from +0.40 V onwards the absorbance decreases, which clearly coincides with the onset potential of the anodic peak recorded in the CV (Fig. S1a). The absorbance continues to decrease until reaching again this potential of +0.40 V in the backward scan. The relationship of the 286 nm absorption band with UA oxidation can be confirmed with the similarity between the evolution of DVA at 286 nm and the CV represented in Fig. S1d, where only the anodic scan is plotted.

3.3. Study of mixtures of OFL and UA using UV–Vis SEC

Once the behavior of each components is identified, the UV–Vis spectroelectrochemical study of a synthetic sample containing the two molecules, OFL and UA, was performed. For this purpose, a solution of 75 μM OFL and 200 μM UA in 0.1 M KCl and BR buffer (pH = 4.02) was prepared. In this case, Fig. 3a shows the CV performed between 0.00 V and +1.10 V at 0.01 $V \cdot s^{-1}$. Two anodic peaks are observed at +0.45 V and +0.96 V related to the oxidation of UA and OFL, respectively.

The evolution of the spectra with the potential during the anodic scan is shown in Fig. 3b, taking the spectrum of the initial solution of UA and OFL as reference. As can be observed, initially a band appears at 287 which shifts up to 294 nm (inset Fig. 3b), indicating that from 0.00 to +0.85 V approximately, only the oxidation of UA is occurring, and from +0.85 V onwards the oxidation of OFL is taking place. Selecting 286 and 294 nm as representative wavelengths for each one of the molecules, it can be seen that the CVAs clearly show changes related to the initial oxidation of UA and the subsequent oxidation of OFL from +0.85 V onwards (Fig. 3c). Both absorption bands are fully overlapped, being difficult to discriminate the absorbance related only to OFL due to the initial presence of UA which is easily oxidized. The same behavior is observed in the DVAs at these two wavelengths that are fully correlated with the electrochemical signal (Fig. 3d). The sample was measured in triplicate. Fig. S2. shows the corresponding CVs and CVAs at 286 and 294 nm. The overlapping between the three measurements demonstrates the good repeatability of the spectroelectrochemical measurements carried out with the new UV–Vis SEC cell, which is also corroborated by the estimation of the %RSD at the vertex potential (+1.10 V), which yields a value around 1 % for the spectroscopic signals and 11 % for the electrochemical response (Table S1).

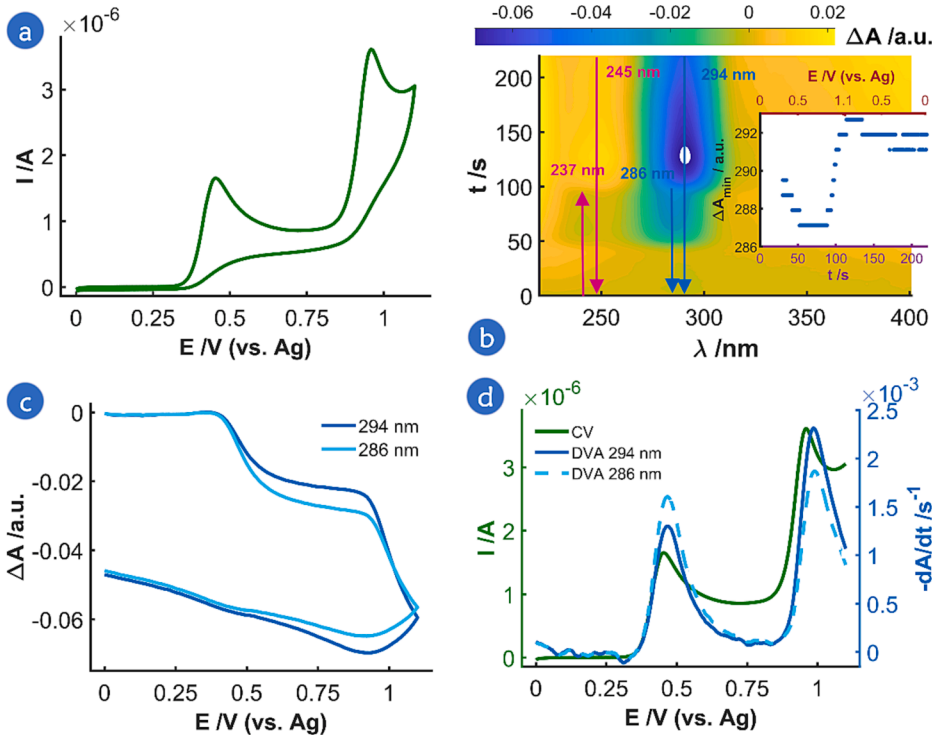

Fig. 3. SEC experiment of 75 μM OFL and 200 μM UA in BR buffer (pH = 4.02) and 0.1 M KCl between 0.00 V and +1.10 V at 0.01 $V \cdot s^{-1}$. (a) CV, (b) contour plot with spectra evolution during the potential scan; inset: wavelength at which the minimum of absorbance is reached during the experiment, (c) CVA at 286 and 294 nm, and (d) comparison of CV and DVA at 286 and 294 nm.

3.4. Study of real urine samples using UV–Vis SEC

Considering that the main objective of this work is to determine OFL in urine samples, the subsequent experiments involved the comparison of the signals acquired from synthetic and urine samples, spiked and non-spiked with OFL and UA. Different test samples, T1, T2, T3 and T4, were prepared as follows. The test urine sample without OFL (T1) contains 0.25 mL of urine in a final volume of 5 mL of BR buffer (pH = 4.02) in 0.1 M KCl. The OFL-enriched urine test sample (T2) was prepared by dissolving 0.00300 g of OFL in 10 mL of urine to simulate a real problem where the concentration of OFL in urine would be 830.18 μM. This test sample was prepared taking into account that the concentration of OFL excreted in urine by a patient taking this drug ranges from 500 to 1250 μM [3]. Next 0.25 mL of this test sample was diluted in 5 mL of BR buffer (pH = 4.02) in 0.1 M KCl, with a final OFL concentration of 41.51 μM. No other pretreatment of the urine sample was carried out. The UA-enriched urine sample (T3) contains 0.25 mL of urine and 73.57 μM UA in a final volume of 5 mL of BR buffer (pH = 4.02) in 0.1 M KCl. The UA-OFL-enriched urine sample (T4) contains a final concentration of 73.57 μM UA, 41.51 μM OFL, 0.25 mL of urine and 0.1 M KCl, all in a final volume of 5 mL of BR.

The CVs of the four samples (Fig. 4a) show a first anodic peak at +0.45 V related to the UA which is present in urine. The same anodic peak is shown in Fig. S1a and Fig. 3a. A second slight oxidation peak overlapped with the one of UA can be observed, which means that other products in the urine besides UA are oxidized around +0.52 V. As can be seen, the UA oxidation peak of the urine samples is broader than in synthetic samples, and its slope is less pronounced than the observed in the oxidation peak of the sample containing only UA and OFL, Fig 3a. Next, a third anodic peak at +0.84 V is observed in the urine samples without OFL (T1 and T3, purple and blue lines, Fig. 4a) which could interfere and difficult the electrochemical OFL quantification in this these medium. On the other hand, the CVs of the urine samples spiked with OFL (T2 and T4, green and orange lines, Fig. 4a) displays the fourth anodic peak at +0.96 V due to the oxidation of OFL added, as explained in Figs. 2a and 3a. Furthermore, this experiment confirms that the first oxidation peak in urine, observable in T1, corresponds to UA, since in T3, where UA is spiked to the sample, the first oxidation peak increases in intensity.

The evolution of the UV-Vis absorption spectra during the oxidation of the molecules present in the urine samples T1 and T2 is shown in Fig. 4b and c. In the sample in which only urine is present (T1, Fig. 4b), the decrease of an absorption band peaking at 286 nm is observed, related to the oxidation of UA, coinciding with the anodic peak at +0.45 V in the CV (T1, purple line, Fig. 4a). This specific oxidation process is clearly observed in the CVA at 291 nm shown in Fig. 4d (purple line), where only the decrease of absorbance is appreciated around +0.45 V. However, in the urine sample spiked with OFL (T2, Fig. 4c) is observed a shifting of the absorption band related to OFL from 286 nm to 291 nm at the end of the potential scan. This behavior is comparable to the spectral evolution illustrated in Fig. 3b for the UA and OFL mixture, demonstrating that the spectral changes observed for solutions T2 and the mixture of 75 μM OFL and 200 μM UA are related to identical processes. UA initially undergoes an oxidation (evidenced by the absorption band at 286 nm), followed by OFL oxidation (absorption band at 291, slightly shifted to shorter wavelengths in the T2 solution). The CVA at 291 nm of T2 solution (green line, Fig. 4d) shows the two anodic processes occurring at +0.45 V and +0.96 V as mentioned for the oxidation of UA and OFL, respectively. T3 sample shows a similar behavior to T1 sample where only the oxidation of UA is observed both in the CV and in the CVA at 291 represented in Fig. 4d (line blue). Lastly, the CVA at 291 of sample T4 (line orange, Fig. 4d) shows a similar behavior to T2, where both the oxidation of UA and OFL is observed.

Samples T1, T2, T3 and T4 were measured three times with the cell developed to perform UV–Vis SEC in order to evaluate de reproducibility. Fig. S3 shows the corresponding CVs, and CVAs at 286 and 291 nm. In addition, %RSD values at +1.10 V were estimated and summarized in Table S2. These results show the good repeatability of the

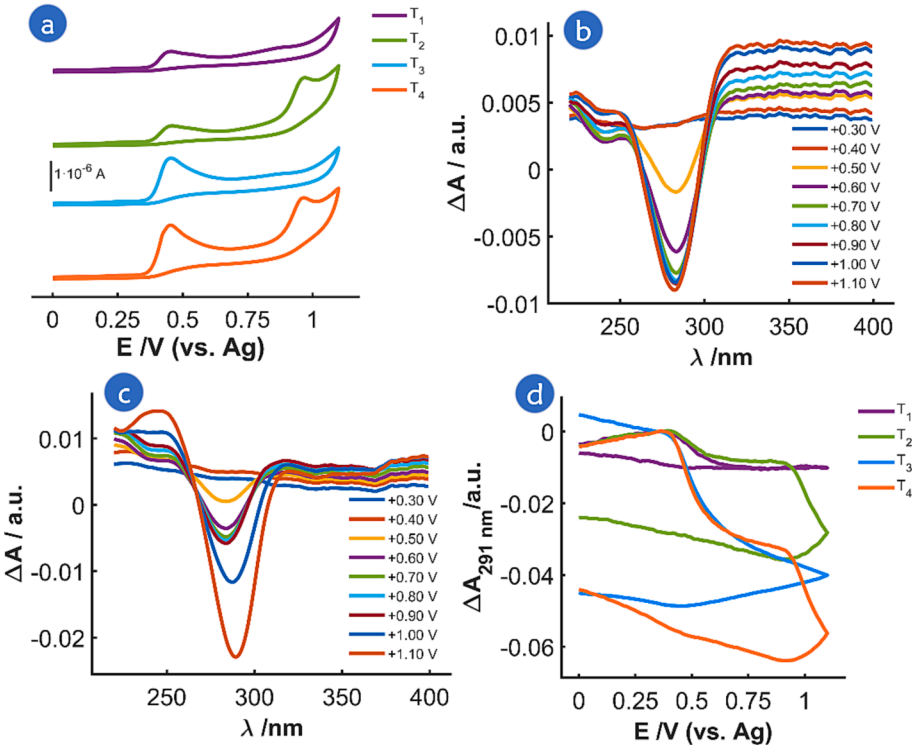

Fig. 4. SEC experiment of T1 (urine), T2 (urine spiked with OFL), T3 (urine spiked with UA) and T4 (urine spiked with OFL and UA) test samples in 0.1 M KCl and in BR buffer (pH = 4.02) between 0.00 V and +1.10 V at 0.01 V·s^{-1}. (a) CVs, (b) spectra evolution during the potential scan of T1, (c) spectra evolution during the potential scan of T2, (d) CVAs at 291 nm.

signals, since in the most of the cases values of %RSD lower than 5 % were obtained.

Two different OFL and urine concentrations are plotted in Fig. S4, demonstrating the well-defined spectroelectrochemical responses obtained in our measurements in linear sweep voltammetry experiments in spite of the presence of interfering compounds in this complex matrix. As can be seen, SEC responses using voltammetry has been demonstrated to be very useful for the comprehension of these complex responses.

3.5. Calibration model to determine OFL in urine matrix samples

The analysis of the spectroelectrochemical signals presented above demonstrates that various oxidation processes could interfere the determination of OFL in urine. In order to control the oxidation process taking place in the urine sample, multipulsed amperometric detection (MAD) was selected as electrochemical technique. For this purpose, a first potential pulse of +0.75 V was applied for 90 s to oxidize and remove from the closest solution to the electrode any interfering component, such as UA. This potential is high enough to oxidize UA but low enough to avoid the oxidation of the OFL. In a second step, a potential pulse of +1.10 V was applied during 90 s to specifically oxidize the target molecule, OFL.

Considering these conditions, calibration samples containing different concentrations of both UA and OFL were prepared to build a calibration model capable of predicting the concentration of OFL in a test urine sample. All these solutions were prepared in BR buffer and 0.1 M KCl (pH = 4.02), randomly varying their concentrations in the range of 10–200 μM, as is shown in Table S3. Additionally, a solution containing only OFL and another containing only UA were also prepared and measured. Finally, the solution with 100 μM OFL and 75 μM UA was selected as test sample and was measured four times to determine the repeatability of the calibration model.

From each experiment, the corresponding multipulse chronoamperogram and the spectra evolution along the two applied potentials were recorded. Fig. S5 shows the signals recorded from experiment E08 (Table S3): the chronoamperogram (CA, Fig. S5a) and the spectra evolution during the two potential steps (Fig. S5b). The obtained spectra after applying a potential of +0.75 V for 90 s displays a weak negative absorption band at 237 nm and a more intense band at 286 nm (Fig. S5b, green lines), which coincides with the spectra previously shown in the UA oxidation during the CV (Fig. S1b). On the other hand, the spectrum obtained after applying a second potential step of +1.10 V for 90 s shows a positive absorption band at 250 nm and a negative band at 292 nm related to OFL consumption in the solution/electrode interface (Fig. S5b, red lines).

Linear calibration models can be assessed with both the electrochemical and the spectroscopic signals for the two analytes, UA and OFL, using the samples indicated in Table S3. The regression parameters obtained with the four calibration models are summarized in Table 1.

The capability of prediction of the OFL calibration models evaluated by measuring four replicates of two OFL-enriched urine samples was very low, with relative errors between 22 % and 67 % for the CA calibration model and between 12 % and 58 % for the spectroscopic calibration model. The overlapping of UA and OFL absorption bands makes difficult the determination of OFL by simple linear regression models. This problem is also evident within the electrochemical calibration model. Although the coefficient of determination is not as low as in the other cases ($R^2 = 0.9773$), the model does not provide enough accuracy to determine OFL in this complex sample.

Table 1
Regression parameters obtained from the 4 linear regression models built with the electrochemical and spectroscopic signals registered with the mixtures of OFL and UA in Table S3.

Molecule	Calibration model	R^2	Sensitivity	S_{yx}
UA (E_{ap} = +0.75 V)	CA: $I_{10\ s}$ *vs.* C_{UA}	0.9553	$9.34 \cdot 10^{-9}$ A·μM^{-1}	$1.14 \cdot 10^{-7}$
	Spectra: $A_{286\ nm,\ 79\ s}$ *vs.* C_{UA}	0.5909	$2.82 \cdot 10^{-4}$ μM^{-1}	$1.34 \cdot 10^{-2}$
OFL (E_{ap} = +1.10 V)	CA: $I_{100\ s}$ *vs.* C_{OFL}	0.9773	$2.80 \cdot 10^{-8}$ A·μM^{-1}	$2.63 \cdot 10^{-7}$
	Spectra: $A_{292\ nm,\ 179\ s}$ *vs.* C_{OFL}	0.9438	$1.28 \cdot 10^{-3}$ μM^{-1}	$1.92 \cdot 10^{-2}$

R^2: Determination coefficient. S_{yx}: residual standard deviation.

Parallel Factor Analysis (PARAFAC) [29] was used to measure OFL levels in urine samples. Given the trilinear character of the time-resolved SEC data, PARAFAC can be used to determine the analyte in complex matrices without any sample pretreatment. Absorbance data at different wavelengths and at different times during a double-pulse chronoamperometric experiments are recorded for mixtures of different OFL and UA concentrations (Table S3), providing a spectroelectrochemistry data cube.

To construct the calibration model with PARAFAC, the cube of data is defined with the values of absorbance from 10 to 175 s, obtained between 225 and 380 nm for all samples. The selected time window corresponds practically to the whole experiment, removing only the initial values of absorbance because of its low value. The wavelengths window belongs to the UV–Vis spectral region where the most significant changes of absorbance occurred, i.e. the selected wavelengths provide all the spectral information about the electrode process. In this way, the data cube is defined by the absorbance values at 1741 times × 196 wavelengths × 14 concentrations. Although the calibration samples contain only two known components (OFL and UA), the PARAFAC model was calculated using three components. The third component could be related to other interfering compounds present in the urine sample. A corcondia value of 96.02 % was obtained for the fitted model. This value indicates that the model constructed is suitable and explains the absorbance changes occurred during the oxidation of the samples shown in Table S3, as the corcondia value is close to 100 % [30].

Fig. 5 illustrates the deconvolution of the spectroelectrochemical data using the PARAFAC model for the samples listed in Table S3. Fig. 5a shows the loadings of the three components obtained with the PARAFAC model plotted versus the wavelength; the spectra of UA (sample E03) and OFL (sample E02) after the oxidation process have also been plotted for comparison. The sign of the absorbance is changed in the experimental spectra to facilitate the comparison. As can be seen, component 1 is fully correlated with UA with a maximum of absorbance at 286 nm, while component 3 is linked with OFL, showing a maximum of absorbance at 294 nm; the spectra are almost identical to the shape of the signals obtained from the loadings of these factors. The loading signal related to the second component is significantly lower than the one of the other two components, but it has been proven to be needed to include this component in order to get a PARAFAC model which explains and fits the spectroelectrochemical data obtained with the set of samples listed in Table S3.

Fig. 5b shows the evolution of the loadings with time during the two applied potential in the experiment; the two chronoabsorptograms at 286 nm for UA (sample E03) and at 294 nm for OFL (sample E02) are overlapped as dotted lines for comparison. Again, the sign of the absorbance has been changed for an easier comparison. As can be observed, the 3rd component assigned to OFL starts to increase when the second potential step is applied, with a value high enough (+1.10 V) to oxidize the OFL; this signal follows a behavior very similar to the chronoabsorptogram registered with the sample E02 prepared only with OFL. On the other hand, the 1st component, ascribed to UA, shows a very similar behavior to the chronoabsorptogram of UA registered for sample E03 which contains only this molecule. As can be observed, the 2nd component is oxidized at the same time than UA, which could be related to any other molecule in this complex sample, being oxidized before the OFL oxidation process.

This PARAFAC model allows the quantification of OFL-enriched urine samples. Two calibration curves were constructed, by

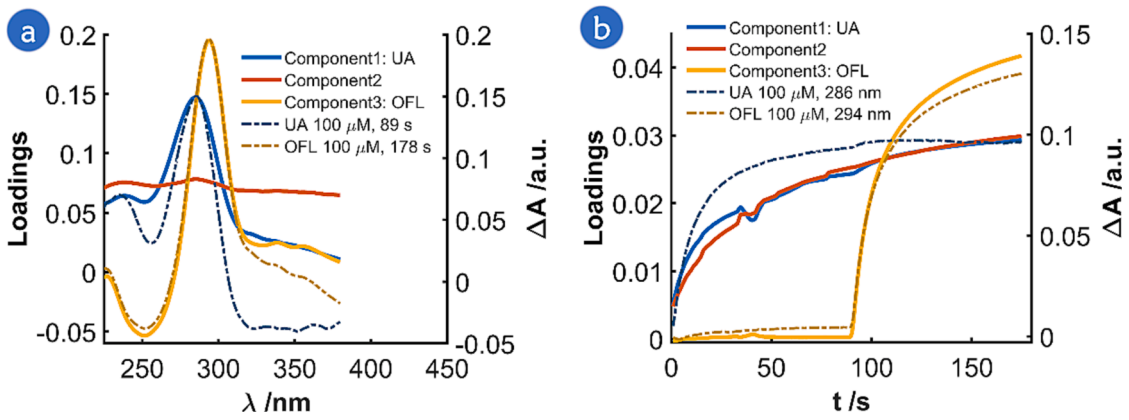

Fig. 5. Loadings of each component obtained with the PARAFAC model versus (a) the wavelength and (b) the time during the double potential step SEC experiments. Solid lines: loadings of the three components versus wavelength (a) and time (b). Dashed lines: UA and OFL spectra (a) and UA and OFL chronoabsorptograms (b) of samples E03 and E02, respectively.

correlating the loadings of the 1st and 3rd component with the concentrations of UA and OFL in the samples listed in Table S3, respectively. The calibration curves and the figures of merit are shown in Fig. S6 and in Table 2, respectively. Least median squares regression was performed to detect outliers, obtaining that the experiment corresponding to sample E04 was an outlier. Once this point is removed a Least Square Regression was performed for the two set of data, loadings of the 3rd component versus OFL concentration (Fig. S6a) and loadings of 1st component versus UA concentration (Fig. S6b).

The figures of merit of the two calibration models obtained indicate the good correlation achieved between loadings of the 3rd component and OFL concentration, with coefficient of determination near 1 (R^2), low residual standard deviation (S_{yx}) and low limit of detection (LOD). However, the UA linear regression model does not supply as good results, with a worse R^2 value and higher S_{yx} and LOD values, indicating that the complexity of the urine matrix affects significantly the UA determination.

Finally, the test OFL-spiked urine sample (T2) was spectroelectrochemically measured following the same MAD protocol described for the mixture samples listed in Table S3. Let us recall that this sample was prepared adding OFL in 10 mL of urine reaching a concentration of 855 μM. Next, this solution was dissolved in 0.1 M KCl and in BR buffer, giving a nominal concentration of 42.75 μM of OFL (T2).

The OFL concentration of this test urine solution was estimated with the PARAFAC calibration model presented in Fig. S6a and Table 2. A very good accuracy is obtained in the prediction of OFL concentration, 41.9 ± 2.5 μM, 98.1 % of recovery with a 3.8 % of relative standard deviation (%RSD) and a relative error of 2.0 %. The %RSD value also indicates that the procedure followed is very repeatable. Therefore, the OFL concentration in the initial solution (T2) is 838 ± 50 μM. These results demonstrate that the PARAFAC model perfectly fulfills the main objective of this work which is the determination of OFL in a test urine sample spiked with this target molecule.

Table 2
Regression parameters obtained from the determination of OFL and UA in mixtures of these molecules with the loadings of the PARAFAC model constructed.

Molecule	Calibration model	R^2	Sensitivity (μM^{-1})	S_{yx}	LOD (μM)
OFL	Loadings component 3 *vs.* C_{OFL}	0.9957	−0.1649	0.66	13.22
UA	Loadings component 1 *vs.* C_{UA}	0.9625	−0.1089	1.22	37.02

R^2: Determination coefficient. S_{yx}: residual standard deviation. LOD: limit of detection.

4. Conclusions

Development of new SEC devices becomes critical because the fields of application of this technique are growing, being chemical analysis one of the most attractive applications for SEC. In this work, we present a new SEC cell that allows the sensitive and reproducible quantification of OFL in urine samples without any pretreatment, only by performing a simple dilution. This SEC cell facilitates the study and quantification of molecules which can modify the WE surface during different oxidation or reduction processes. In this work, the matrix of all the test solutions was urine, which has not been previously pretreated. The different interfering compounds present in urine affect the electrochemical and/or spectroscopic determination of OFL when only univariate models are used. To overcome this drawback, multivariate statistical tools have been used, selecting in this case PARAFAC as the best tool to determine OFL in urine samples. The fitted PARAFAC model has allowed us to properly deconvolve the contribution of OFL and UA to the global SEC signal. Once this objective was achieved, the determination of OFL has been carried out by correlating the loadings of one of the components of the PARAFAC model with the OFL concentration, yielding very good figures of merit. From these results, it can be deduced that the combination of the sensitivity and reproducibility of a good SEC cell and setup, with the specificity of the spectroscopic methods when the test molecule participates in an electrochemical reaction, even in a complex matrix, leads to develop useful, versatile and reliable methods to quantify urinary biomarkers.

CRediT authorship contribution statement

Fabiola Olmo: Writing – review & editing, Writing – original draft, Methodology, Investigation, Formal analysis, Data curation, Conceptualization, Validation, Visualization. **Alvaro Colina:** Writing – review & editing, Writing – original draft, Visualization, Validation, Supervision, Project administration, Methodology, Investigation, Funding acquisition, Formal analysis, Conceptualization. **Aranzazu Heras:** Writing – review & editing, Writing – original draft, Supervision, Resources, Project administration, Methodology, Funding acquisition, Formal analysis, Conceptualization, Investigation, Validation, Visualization.

Declaration of competing interest

The authors declare that they have no known competing financial interests or personal relationships that could have appeared to influence the work reported in this paper.

Data availability

Data will be available in the University of Burgos data repository

Acknowledgments

Ministerio de Ciencia e Innovación and Agencia Estatal de Investigación (Grant numbers: MCIN/AEI/10.13039/501100011033, PID2020-113154RB-C21), Ministerio de Ciencia, Innovación y Universidades (Grant number: RED2022-134120-T), Junta de Castilla y León and European Regional Development Fund (Grant number: BU036P23) are gratefully acknowledged for funding this work. F.O. acknowledges Junta de Castilla y León and European Social Found for his predoctoral contract.

Appendix A. Supplementary data

Supplementary data to this article can be found online at https://doi.org/10.1016/j.microc.2024.110186.

References

[1] J. Li, Q. Xue, T. Chen, F. Liu, Q. Wang, C. Chang, X. Lu, T. Zhou, O. Niwa, The influence mechanism of the molecular structure on the peak current and peak potential in electrochemical detection of typical quinolone antibiotics, Phys. Chem. Chem. Phys. 23 (2021) 13873–13877, https://doi.org/10.1039/d1cp01358k.
[2] L. Riaz, T. Mahmood, A. Khalid, A. Rashid, M.B. Ahmed Siddique, A. Kamal, M. S. Coyne, Fluoroquinolones (FQs) in the environment: A review on their abundance, sorption and toxicity in soil, Chemosphere 191 (2018) 704–720, https://doi.org/10.1016/j.chemosphere.2017.10.092.
[3] J.I. Alós, Quinolonas, Enferm. Infecc. Microbiol. Clin. 27 (2009) 290–297, https://doi.org/10.1016/j.eimc.2009.03.001.
[4] T. Kloskowski, S. Frąckowiak, J. Adamowicz, K. Szeliski, M. Rasmus, T. Drewa, M. Pokrywczyńska, Quinolones as a potential drug in genitourinary cancer treatment—a literature review, Front. Oncol. 12 (2022) 1–14, https://doi.org/10.3389/fonc.2022.890337.
[5] N.G. Bush, I. Diez-Santos, L.R. Abbott, A. Maxwell, Quinolones: mechanism, lethality and their contributions to antibiotic resistance, Molecules 25 (2020) 5662, https://doi.org/10.3390/molecules25235662.
[6] P.C. Appelbaum, P.A. Hunter, The fluoroquinolone antibacterials: past, present and future perspectives, Int. J. Antimicrob. Agents. 16 (2000) 5–15, https://doi.org/10.1016/S0924-8579(00)00192-8.
[7] A. Wong, T.A. Silva, F.C. Vicentini, O. Fatibello-Filho, Electrochemical sensor based on graphene oxide and ionic liquid for ofloxacin determination at nanomolar levels, Talanta 161 (2016) 333–341, https://doi.org/10.1016/j.talanta.2016.08.035.
[8] X. Si, Y. Wei, C. Wang, L. Li, Y. Ding, A sensitive electrochemical sensor for ofloxacin based on a graphene/zinc oxide composite film, Anal. Methods 10 (2018) 1961–1967, https://doi.org/10.1039/c8ay00127h.
[9] T. Liu, Q. Xue, J. Jia, F. Liu, S. Zou, R. Tang, T. Chen, J. Li, Y. Qian, New insights into the effect of pH on the mechanism of ofloxacin electrochemical detection in aqueous solution, Phys. Chem. Chem. Phys. 21 (2019) 16282–16287, https://doi.org/10.1039/c9cp03486b.
[10] Y. Pi, J. Feng, M. Song, J. Sun, Degradation potential of ofloxacin and its resulting transformation products during Fenton oxidation process, Chinese Sci. Bull. 59 (2014) 2618–2624, https://doi.org/10.1007/s11434-014-0293-7.
[11] L. Zhu, B. Santiago-Schübel, H. Xiao, H. Hollert, S. Kueppers, Electrochemical oxidation of fluoroquinolone antibiotics: mechanism, residual antibacterial activity and toxicity change, Water Res. 102 (2016) 52–62, https://doi.org/10.1016/j.watres.2016.06.005.
[12] B.O. Orimolade, A.O. Oladipo, A.O. Idris, F. Usisipho, S. Azizi, M. Maaza, S. L. Lebelo, B.B. Mamba, Advancements in electrochemical technologies for the removal of fluoroquinolone antibiotics in wastewater: a review, Sci. Total Environ. 881 (2023) 163522, https://doi.org/10.1016/j.scitotenv.2023.163522.
[13] L.S. Redgrave, S.B. Sutton, M.A. Webber, L.J.V. Piddock, Fluoroquinolone resistance: mechanisms, impact on bacteria, and role in evolutionary success, Trends Microbiol. 22 (2014) 438–445, https://doi.org/10.1016/j.tim.2014.04.007.
[14] M. Elfiky, N. Salahuddin, A. Hassanein, A. Matsuda, T. Hattori, Detection of antibiotic Ofloxacin drug in urine using electrochemical sensor based on synergistic effect of different morphological carbon materials, Microchem. J. 146 (2019) 170–177, https://doi.org/10.1016/j.microc.2018.12.034.
[15] F. Wu, F. Xu, L. Chen, B. Jiang, W. Sun, X. Wei, Cuprous oxide/nitrogen-doped graphene nanocomposites as electrochemical sensors for ofloxacin determination, Chem. Res. Chinese Univ. 32 (2016) 468–473, https://doi.org/10.1007/s40242-016-5367-4.
[16] N. Manjula, S. Pulikkutty, T.-W. Chen, S.-M. Chen, X. Liu, Hexagon prism-shaped cerium ferrite embedded on GC electrode for electrochemical detection of antibiotic drug ofloxacin in biological sample, Colloids Surf. A Physicochem. Eng. Asp. 627 (2021) 127129, https://doi.org/10.1016/j.colsurfa.2021.127129.
[17] Z. Jiang, G. Li, M. Zhang, A novel electrochemical sensor based on SH-β-cyclodextrin functionalized gold nanoparticles/reduced-graphene oxide nanohybrids for ultrasensitive electrochemical sensing of acetaminophen and ofloxacin, Int. J. Electrochem. Sci. 12 (2017) 5157–5173, https://doi.org/10.20964/2017.06.28.
[18] Y. Yu, F. Huang, Y. He, X. Liu, C. Song, Y. Xu, Y. Zhang, Heterogeneous fenton-like degradation of ofloxacin over sludge derived carbon as catalysts: mechanism and performance, Sci. Total Environ. 654 (2019) 942–947, https://doi.org/10.1016/j.scitotenv.2018.11.156.
[19] X. Liu, F. Huang, Y. Yu, P. Zhao, Y. Zhou, Y. He, Y. Xu, Y. Zhang, Ofloxacin degradation over Cu–Ce tyre carbon catalysts by the microwave assisted persulfate process, Appl. Catal. B Environ. 253 (2019) 149–159, https://doi.org/10.1016/j.apcatb.2019.04.047.
[20] R. Kaur, J.P. Kushwaha, N. Singh, Electro-oxidation of Ofloxacin antibiotic by dimensionally stable Ti/RuO2 anode: evaluation and mechanistic approach, Chemosphere 193 (2018) 685–694, https://doi.org/10.1016/j.chemosphere.2017.11.065.
[21] J. Garoz-Ruiz, C. Guillen-Posteguillo, A. Heras, A. Colina, Simplifying the assessment of parameters of electron-transfer reactions by using easy-to-use thin-layer spectroelectrochemistry devices, Electrochem. Commun. 86 (2018) 12–16, https://doi.org/10.1016/j.elecom.2017.11.001.
[22] J. Garoz-Ruiz, J.V. Perales-Rondon, A. Heras, A. Colina, Spectroelectrochemical sensing: current trends and challenges, Electroanalysis. 31 (2019) 1254–1278, https://doi.org/10.1002/elan.201900075.
[23] J. Garoz-Ruiz, A. Heras, A. Colina, Direct Determination of Ascorbic acid in a grapefruit: paving the way for in vivo spectroelectrochemistry, Anal. Chem. 89 (2017) 1815–1822, https://doi.org/10.1021/acs.analchem.6b04155.
[24] C.A. Schneider, W.S. Rasband, K.W. Eliceiri, NIH Image to ImageJ: 25 years of image analysis, Nat. Methods 9 (2012) 671–675, https://doi.org/10.1038/nmeth.2089.
[25] S.M. Abd El-Hamid, S.A. Sadeek, W.A. Zordok, W.H. El-Shwiniy, Synthesis, spectroscopic studies, DFT calculations, cytotoxicity and antimicrobial activity of some metal complexes with ofloxacin and 2,2′-bipyridine, J. Mol. Struct. 1176 (2019) 422–433, https://doi.org/10.1016/j.molstruc.2018.08.082.
[26] G.M. Park, Hyeong Ryun, Gwang Yeong Jeong, Hyeong Cheol Lee, Jin Gi Lee, G. Baek, Ionization and divalent cation complexation of quinolone antibiotics in aqueous solution, Ioniz. Complexation Quinolone 21 (2000) 849–854, https://doi.org/10.5012/bkcs.2000.21.9.849.
[27] F. Olmo, J. Garoz-Ruiz, A. Colina, A. Heras, Derivative UV/Vis spectroelectrochemistry in a thin-layer regime: deconvolution and simultaneous quantification of ascorbic acid, dopamine and uric acid, Anal. Bioanal. Chem. 412 (2020) 6329–6339, https://doi.org/10.1007/s00216-020-02564-1.
[28] J.L. Owens, H.A. Marsh, G. Dryhurst, Electrochemical oxidation of uric acid and xanthine. An investigation by cyclic voltammetry, double potential step chronoamperometry and thin-layer spectroelectrochemistry, J. Electroanal. Chem. 91 (1978) 231–247, https://doi.org/10.1016/S0022-0728(78)80103-X.
[29] R. Bro, PARAFAC. Tutorial and applications, Chemom. Intell. Lab. Syst. 38 (1997) 149–171, https://doi.org/10.1016/S0169-7439(97)00032-4.
[30] R. Bro, H.A.L. Kiers, A new efficient method for determining the number of components in PARAFAC models, J. Chemom. 17 (2003) 274–286, https://doi.org/10.1002/cem.801.